Deuterium abundance in the interstellar medium: Six new targets observed with *FUSE*

G. Hébrard[1], S. D. Friedman[2], C. M. Oliveira[3], T. Tripp[4], P. Chayer[3,5], A. Lecavelier des Étangs[1], J. Dupuis[6,3], H. W. Moos[3], A. Vidal-Madjar[1]

1: Institut d'Astrophysique de Paris, UMR7095 CNRS, Université Pierre & Marie Curie, 98bis boulevard Arago, F-75014 Paris, France.
2: Space Telescope Science Institute, 3700 San Martin Drive, Baltimore, MD 21218, USA.
3: Department of Physics & Astronomy, The Johns Hopkins University, Baltimore, MD 21218, USA.
4: Department of Astronomy, University of Massachusetts, Amherst, MA 01003, USA.
5: Department of Physics & Astronomy, University of Victoria, Victoria, BC V8W 3P6, Canada.
6: Canadian Space Agency, 6767 route de l'Aéroport, Saint-Hubert, QC J3Y 8Y9, Canada.

January 2006
Contact: hebrard@iap.fr

Abstract

We present deuterium abundance analyses of the 905–1187 Å spectra obtained with the Far Ultraviolet Spectroscopic Explorer (*FUSE*) toward six new lines of sight: the hot DA white dwarf WD 1528+487 and DAO white dwarf WD 2011+395, the hot subdwarf O stars LB 1566, LSE 263, and LSE 234, and the B dwarf star HD 206773. Numerous interstellar lines are detected on the continuum of the stellar spectra. Analyses were performed through the simultaneous fits of interstellar absorption lines, including H I, D I, O I, N I, P II, Fe II, Si II, H_2, and HD. Curve of growth analyses and archival STIS data were also used. We report preliminary interstellar abundances along these sight lines and compare them with those obtained toward other targets. D/O might be considered to be a good proxy for D/H but surprisingly, D/H shows a larger dispersion than D/O does. However, our new targets seem to show more dispersion in D/O that it was seen before. These results might suggest concerns on f-values or possible blends with some O I lines.

1 Introduction

Deuterium is supposed to be produced during primordial nucleosynthesis and then destroyed by astration. Whereas measurements in low-metallicity QSO absorption systems probe $(D/H)_{primordial}$, the present epoch deuterium abundance $(D/H)_{PE}$ can be measured in the interstellar medium.

$(D/H)_{ISM}$ likely has a single value in the Local Bubble, in the range $[1.3-1.6]\times10^{-5}$ (Moos et al. 2002, Hébrard & Moos 2003, Wood et al. 2004). However, it now appears that this local abundance should not be considered as a canonical value characteristic of the Milky Way at the present epoch. Indeed, numerous distant sight lines have shown deuterium abundances in disagreement with it.

Hébrard & Moos (2003) and Wood et al. (2004) have shown that the deuterium abundance is lower for the most distant sight lines than in the Local Bubble. While Hébrard & Moos (2003) suggested $(D/H)_{PE}$ would be significantly lower than 1×10^{-5}, Linsky et al. (2006) proposed a $(D/H)_{PE}$ ratio higher than 2×10^{-5} assuming that deuterium could be significantly depleted onto dust grains.

The size of the sample of sight lines analyzed so far, especially the distant ones, prohibits strong conclusions to be drawn. Here we present deuterium abundance analyses toward six new lines of sight observed with *FUSE*. We compare the D/H and D/O ratios of those sight lines with those obtained toward other targets, as well as other ratios, including $O/H = (3.43\pm0.15)\times10^{-4}$ (Meyer 2001), $N/H = (7.5\pm0.4)\times10^{-5}$ (Meyer et al. 1997), or $\log$ P II/O I $= -3.26^{+0.12}_{-0.10}$ (Lebouteiller et al. 2005).

2 Observations and data processing

The *FUSE* observations used in this study were performed as part of Science Team D/H programs (P204, P205, and P302), Calibration program (M105), and Guest Investigator programs (B071, D058, D066, and E045). Table 1 and 2 summarize relevant sight line and atmospheric parameters for the six targets and observing log.

The spectra were extracted from the detector images and calibrated using the CalFUSE pipeline. The individual exposures were averaged separately for each channel (SiC1, SiC2, LiF1, and LiF2) and each available slit (MDRS and/or LWRS), after correcting for zero-point wavelength offsets between individual exposures. *FUSE* spectra samples of the six targets are plotted in Figure 1.

3 Description of the spectra

WD 1528+487 and WD 2011+395 are two white dwarfs. The stellar continua present mainly H I Lyman series, with few metal lines (C, O, Si, S, P) in the case of WD 2011+395. Except for those few features, most of the lines are due to interstellar absorptions. No He II lines are seen in the *FUSE* spectra of those white dwarfs. Note however that WD 2011+395 shows the optical He II line at λ 4686 Å, that makes it a DAO-type white dwarf, whereas WD 1528+487 is a pure DA. Due to their simple stellar continua and high UV fluxes, white dwarf targets are particularly well suited for interstellar abundances measurements at the hundred-parsec scale. Such kind of targets were largely used to measure deuterium abundance within the Local Bubble with *FUSE* (see, e.g., Moos et al. 2002, Hébrard & Moos 2003, Oliveira et al. 2003).

LB 1566, LSE 263, and LSE 234 are sdO stars. Unlike the white dwarfs, they present plenty of photospheric features blended with interstellar lines. Less abundant but brighter in the UV than white dwarfs, subdwarfs allow interstellar abundances measurements at the scale of several hundreds parsecs. Several *FUSE* measurements of

deuterium were performed using those targets (see, e.g., Friedman et al. 2002, 2006, Hébrard & Moos 2003, Wood et al. 2004). The uncertainties in the stellar continua might be a source of systematic errors because of the blends between interstellar and unidentified stellar lines (due to lack of atomic data). This might be particularly true for D I, whose lines are all blended with stellar He II lines, that are seen in the *FUSE* spectra of the three subdwarfs. Note that LSE 234 shows a strong P Cyg O VI profile around λ 1035 Å.

The last target, HD 206773, is a hot B star. OB stars allow interstellar medium to be probed at the thousand-parsec scale. *FUSE* deuterium measurements towards three OB stars were published for three targets up to now (Hoopes et al. 2003, Hébrard et al. 2005). Numerous interstellar molecular hydrogen lines are seen. Such kind of blends are a less severe issue than stellar blends, as the interstellar H_2 content of the line of sight is easier to model.

4 Data analysis

Column densities (N) have been measured from the analyses of the interstellar lines detected on the six lines of sight, using the method presented by Hébrard et al. (2002). The numerous absorption lines detected on the four *FUSE* channels and through the one or two available slits were fitted simultaneously by Voigt profiles. The parameters of the interstellar clouds (column densities, radial velocities, temperatures, and turbulent velocities) are free to vary, as well as the continua (polynomials), the widths of the Gaussian line spread function, or some wavelength scale shifts.

As far as possible, we excluded saturated lines in order to reduce possible systematic errors on the column density measurements. A curve of growth (COG) analysis was also performed for one target, following the method described by Oliveira et al. (2003). H I column densities were measured from *FUSE* or HST data in the cases of

LB 1566, LSE 234, and HD 206773. N(H I) values from the literature are used for the three remaining targets; they remain however uncertain. The wavelengths and oscillator strengths (f-values) used in the analysis are from Morton (2003) for atoms and ions, from Abgrall et al. (1993a, 1993b) for H_2, and from Abgrall & Roueff (2005) for HD.

5 Results

The preliminary column densities and the derived ratios are reported in Table 3. We discuss below the six individual targets. Some examples of fits are plotted in Figure 2.

5.1 WD 1528+487

Numerous unsaturated D I, O I, or N I lines are available in the *FUSE* spectra of WD 1528+487. The D I lines are detected in the blue wings of several Lyman lines but they are not well resolved. There are no damping wings of the H I lines seen in the *FUSE* bandpass and no Lyman-α observations are available for this target. The only N(H I) measurement available is from EUV flux observed with ROSAT (Marsh et al. 1997), which is model-dependent. One can suspect a significant underestimation of N(H I) as the D/H, O/H, and N/H ratios are all three about one order of magnitude larger than those usually observed in the interstellar medium. This might indicate the need to reconsider the stellar models.

WD 1528+487 is probably located within the Local Bubble. However, the D/O ratio on this sight line is in marginal agreement with the Local Bubble value. The P II/O I ratio is in good agreement with this observed toward other lines of sight.

The LWRS data of WD 1528+487 were previously analyzed by Lehner et al. (2003), who reported the detection of two interstellar components, with a radial velocity separation of 40 km/s. We did not detect the weak component. Our O I and P II measurements are

in good agreement with those of Lehner et al. (2003), whereas the agreement is marginal for N I and poor for Fe II and Si II.

5.2 WD 2011+395

Numerous unsaturated lines are also available for this sight line, for atoms, ions, and molecules. The D I lines are well resolved. Marsh et al. (1997) derived $\log N(\mathrm{H\,I}) = 19.61^{+0.12}_{-0.17}$ from EUV flux observed with ROSAT, which implies O/H and N/H ratios in good agreement with those observed in the interstellar medium. This led us to adopt this value. This measurement is however model-dependent. Thorstensen et al. (1994) estimated $\log N(\mathrm{H\,I})$ in the range $[18.78 - 19.15]$ using the same data, and they estimated $\log N(\mathrm{H\,I})$ in the range $[19.0 - 19.4]$ from EUVE data. Such differences might illustrate the uncertainties of these measurements. The analysis of the atmosphere of WD 2011+395 based on the *FUSE* and EUVE spectra will improve the determination of $N(\mathrm{H\,I})$.

Both D/O and D/H appear to be high, which makes this sight line a good candidate for a high deuterium abundance. The P II/O I ratio is low; decreasing $N(\mathrm{O\,I})$ in order to make that ratio in better agreement with other sight lines would make the D/O ratio even larger.

The first *FUSE* data of WD 2011+395 were analyzed with COGs by Lehner et al. (2003), who reported results in agreement with ours. An exception is O I: Lehner et al. (2003) reported $\log N(\mathrm{O\,I}) = 16.06^{+0.06}_{-0.05}$. The COG analysis we performed confirmed however the results we obtained from profile fitting (see Figure 3).

5.3 LB 1566

As column densities start to be high, fewer unsaturated lines are available here. This is particularly an issue in the case of O I, for which only one unsaturated transition is available: $\lambda\,974$ Å. Hébrard et al. (2005) concluded that $\lambda\,974$ Å presents no strong oscillator strength inconsistencies nor significant uncontrolled blends. The

D/O ratio is low, and about four times lower than the one measured toward the two white dwarfs.

The high column density allows Lyman-β damping wings to be fitted in order to measure N(H I). Most of the error on N(H I) depends on the uncertainty in the stellar continuum. We used polynomials of different orders to model it. The obtained D/H is low; this seems to confirm, together with the low D/O, the low deuterium abundance of this line of sight.

5.4 LSE 263

This subdwarf shows numerous stellar lines, most of them being unidentified. Several interstellar lines are not well fitted, probably because of uncontrolled blend. This is the case for λ 974 Å. As this line is the only unsaturated one available with *FUSE*, N(O I) is particularly uncertain. Diplas & Savage (1994) measured N(H I) using Lyman-α IUE observations of LSE 263. Because the stellar continuum of this target is not well modeled, the measured interstellar column densities might be doubtful.

5.5 LSE 234

Due to the high column density, only a few unsaturated lines are available: three Lyman lines for D I, λ 974 Å for O I, and the N I multiplet at λ 955 Å. N(H I) has been determined with the damped profile of the Lyman-β line. The error on it is mainly due to uncertainties in the stellar continuum (modeled by polynomials). Our result is fully consistent with the determination done by Diplas & Savage (1994) with IUE observations of the Lyman-α line. We note that the N(O I) from λ 974 Å is consistent with λ 922.2 Å but not with λ 919.9 Å (both O I lines are likely to be saturated). Similar trends were already found for Feige 110 (Hébrard et al. 2005) and LSE 44 (Friedman et al. 2006); this might be hints for oscillator strength values and/or blends issues.

The D/H ratio of this target located outside the Local Bubble is particularly high. D/O is similar to the Local Bubble value, which makes the D/O toward LSE 234 the highest measured up to now in this high column density range.

5.6 HD 206773

N(H I) toward HD 206773 was measured with a STIS spectrum (a 360 s snapshot performed with E140H). We fitted the damped Lyman-α profile applying the procedure described in Jenkins et al. (1999) and Sonneborn et al. (2000). Here again, the error on N(H I) is dominated by the continuum placement uncertainty. Our result agrees with Grillo et al. (1992), who reported $\log N(\mathrm{H\,I}) = 21.5$ from from visual extinction. Figure 4 shows some STIS data samples.

Such a high column density produces particularly severe saturation problems. Even the highest D I line detected in the Lyman series (λ 916.2 Å) seems strongly saturated (optical depth $\tau \simeq 15$). All the UV flux is absorbed at shorter wavelengths. Accurate measurement of N(D I) on this sight line seems jeopardized. Constraining the velocity structure of this sight line with high spectral resolution data might however help. Up to now, the highest D I column densities measured from UV absorption lines are around 16.2 dex (Hébrard et al. 2005, Oliveira et al. 2006a).

The STIS data also allowed N(O I) to be accurately measured from direct integration of the weak λ 1356 Å line (assuming that the line is not affected by unresolved saturation). The result (17.85 ± 0.05) is slightly higher the one obtained from *FUSE* with λ 974 Å (17.67 ± 0.15). However, according to the error bars, there is no significant signature of f-value inconsistency between those two lines. Hébrard et al. (2005) have shown the good agreement between them in the case of HD 195965.

N(N I) can be accurately measured with *FUSE* in this high column density regime thanks to the weak doublet at λ 1160 Å.

6 Discussion

Previous studies of the O/H abundance support the view that oxygen should be a good proxy for hydrogen (Meyer et al. 1998; André et al. 2003; Cartledge et al. 2004; Oliveira et al. 2005). Thus, D/O might be considered to be a good proxy for D/H, which is particularly sensitive to astration and which may be less sensitive to systematic effects (Timmes et al. 1997; Hébrard & Moos 2003).

Figure 5 shows D/O and D/H as a function of the D I column density. As discussed by Hébrard et al. (2005), D/H shows a larger dispersion than D/O does. This discrepancy is puzzling and difficult to understand if oxygen really is a good hydrogen proxy. This might call into question the O/H homogeneity.

However, our new targets seem to show more dispersion in D/O that it was seen before. Indeed, WD 1528+487 and WD 2011+395 show D/O ratios around 6.5×10^{-2}, which is significantly higher than the homogeneous ratio measured within the Local Bubble, $(\mathrm{D/O})_{\mathrm{LB}} = (3.84 \pm 0.16) \times 10^{-2}$ (Hébrard & Moos 2003). Moreover, the distant target LSE 234 shows a D/O ratio significantly higher than the distant D/O, $(1.75 \pm 0.18) \times 10^{-2}$ (Hébrard et al. 2005). This might be signatures of D/O variations.

WD 1528+487 and WD 2011+395 present the highest D/O ratios on the plot. It should be noted that the weak O I line at 974 Å is detected toward none of them. Oliveira et al. (2006b) and Dupuis et al. (2006) report also targets with high D/O ratios, without λ 974 Å detections. Hébrard et al. (2005) and Friedman et al. (2006) warn against not using this O I line which may lead to an underestimation of N(O I), thus to an overestimation of D/O. The lack of detection of this O I line on these sight lines is both due to the low column density and the low signal-to-noise ratio. Significantly longer exposures might help to resolve this problem.

On the other hand, all the distant targets that show low D/O ratios are based on λ 974 Å and/or λ 1356 Å O I lines measurements. It is notable that most of those based on λ 974 Å only present a high O/H ratio. All of these might suggest concerns on f-values or possible blends with some O I lines. This issue should be further explored. Available *FUSE* and HST archive data might be used for that.

This work is based on observations made with the NASA-CNES-CSA Far Ultraviolet Spectroscopic Explorer. The *FUSE* mission is operated for NASA by the Johns Hopkins University. Financial support to U. S. participants has been provided by NASA contract NAS5-32985. French participants are supported by CNES. This work has been done using the profile fitting procedure Owens.f developed by M. Lemoine and the *FUSE* French Team.

References:

Abgrall, H., Roueff, E., Launay, F. et al. 1993a, A&AS, 101, 273
Abgrall, H., Roueff, E., Launay, F. et al. 1993b, A&AS, 101, 323
Abgrall, H., & Roueff, E. 2005, A&A, 445, 361
André, M. K., Oliveira, C. M., Howk, J. C. et al. 2003, ApJ, 591, 1000
Cartledge, S. I. B., Lauroesch, J. T., Meyer, D. M., & Sofia, U. J. 2004, ApJ, 613, 1037
Diplas, A., & Savage, B. 1994, ApJS, 93, 211
Dupuis, J., Oliveira, C., Hébrard, G. 2006, AAS 207th Meeting, poster 175.18
Friedman, S. D., Howk, J. C., Chayer, P. et al. 2002, ApJS, 140, 37
Friedman, S. D. et al. 2006, ApJ Feb 2006 (astro-ph/0510593) & AAS 207th Meeting, poster 175.04
Grillo, F., Sciortino, S., Micela, G. et al. 1992, ApJS, 81, 795
Hébrard, G., Lemoine, M., Vidal-Madjar, A. et al. 2002, ApJS, 140, 103
Hébrard, G., & Moos, H. W. 2003, ApJ, 599, 297
Hébrard, G., Tripp, T. M., Chayer, P. et al. 2005, ApJ, 635, 1136
Hoopes, C. G., Sembach, K. R., Hébrard, G. et al. 2003, ApJ, 586, 1094
Jenkins, E. B., Tripp, T. M., Wozniak, P. R., et al. 1999, ApJ, 520, 182
Lebouteiller, V., Kuassivi, & Ferlet, R. 2005, A&A, 443, 509
Lehner, N., Jenkins, E. B., Gry, C. et al. 2003, ApJ, 595, 858
Linsky, J. L., Draine, B. T , Moos, H. W. et al. 2006, AAS 207th Meeting, poster 175.03
Marsh, M. C., Barstow, M. A., Buckley, D. A. et al. 1997, MNRAS, 287, 705
Meyer, D. M., Cardelli, J. A., & Sofia, U. J. 1997, ApJL, 490, L103
Meyer, D. M., Jura, M., & Cardelli, J. A. 1998, ApJ, 493, 222
Meyer, D. M. 2001, XVIIth IAP Colloquium, Paris, Edited by R. Ferlet et al., p. 135
Moos, H. W., Sembach, K. R., Vidal-Madjar, A. et al. 2002, ApJS, 140, 3
Morton, D. C. 2003, ApJS, 149, 205
Oliveira, C. M., Hébrard, G., Howk, J. C. et al. 2003, ApJ, 587, 235

Oliveira, C. M., Dupuis, J., Chayer, P., Moos, H. M. 2005, ApJ, 625, 232
Oliveira, C. M., Moos, H. W., Hébrard, G., Knauth, D. 2006a, AAS 207th Meeting, poster 175.07
Oliveira, C. M., Moos, H. W., Chayer, P., Kruk, J. W. 2006b, ApJ, in press
Sonneborn, G., Tripp, T. M., Ferlet, R. et al. 2000, ApJ, 545, 277
Thorstensen, J. R., Vennes, S., Shambrook A. 1994, AJ, 108, 1924
Timmes, F. X., Truran, J. W., Lauroesch, J. T., & York, D. G. 1997, ApJ, 476, 464
Wood, B. E., Linsky, J. L., Hébrard, G. et al. 2004, ApJ, 609, 838

Table 1: Targets.

Target	WD 1528+487	WD 2011+395	LB 1566	LSE 263	LSE 234	HD 206773
Sp. type	DA1	DAO (+M3)	sdO	sdO	sdO	B0V:pne
RA (2000)	15 29 43.5	20 13 09.8	00 40 13.3	19 02 11.8	18 13 15.8	21 42 24.2
DEC (2000)	+48 36 25	+40 02 41	−55 01 52	−51 30 10	−64 55 17	+57 44 10
$l^{\rm II}$ (°)	78.9	77.0	306.4	345.2	329.4	99.8
$b^{\rm II}$ (°)	+52.7	+3.2	−62.0	−22.5	−20.5	+3.6
d (pc)	140[a]	141[a]	...	...	460 ± 120[a]	500^{+200}_{-120}[b]
V	14.7	14.6	13.1	11.3	12.6	6.9
$\log g$	7.77	7.74	...	...	...	...
$T_{\rm eff}$ (K)	47600	53600	...	...	...	29600

[a] Photometric.

[b] From *Hipparcos* parallaxe.

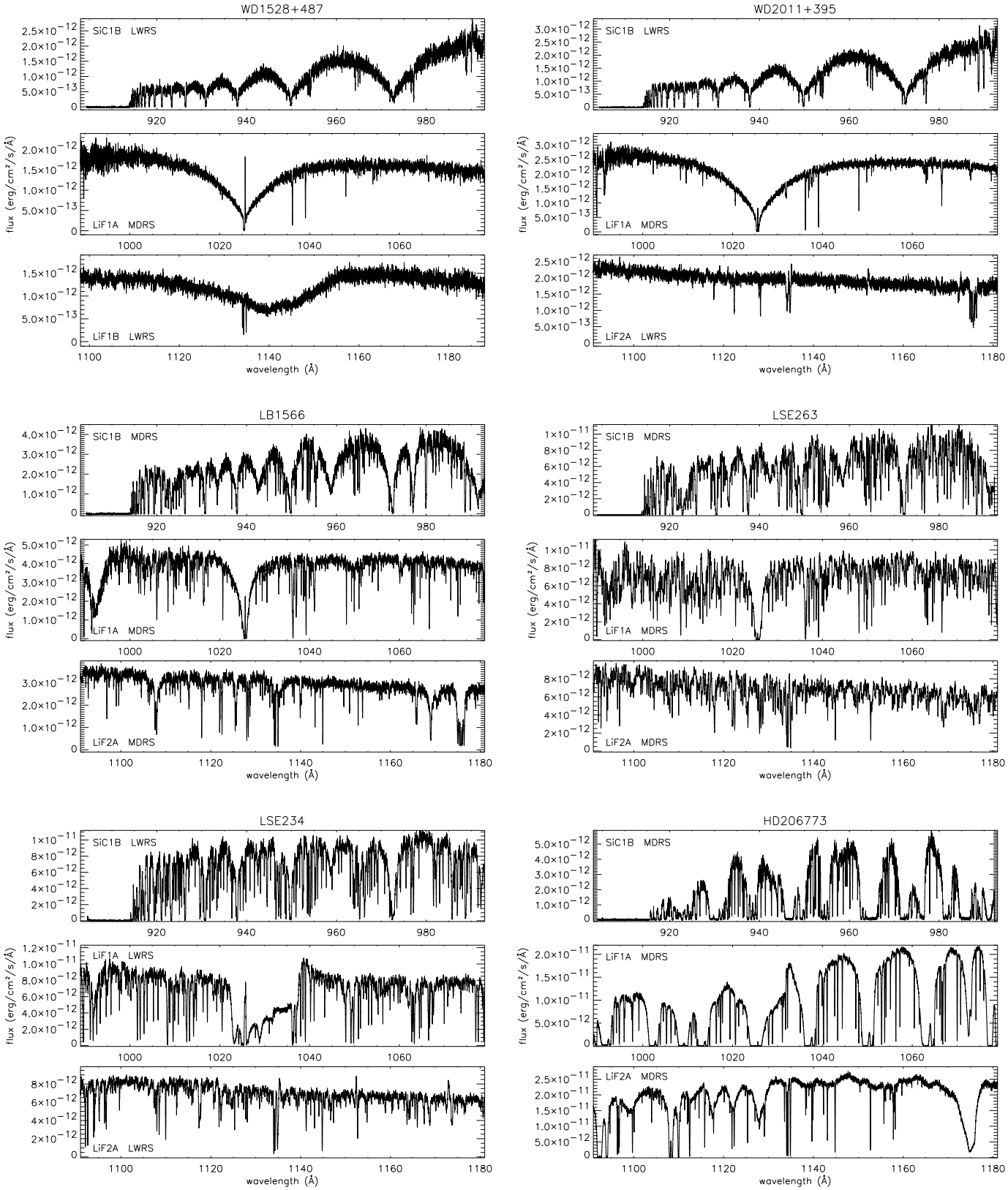

Figure 1: Samples of the *FUSE* spectra of the six targets.

WD 1528+487

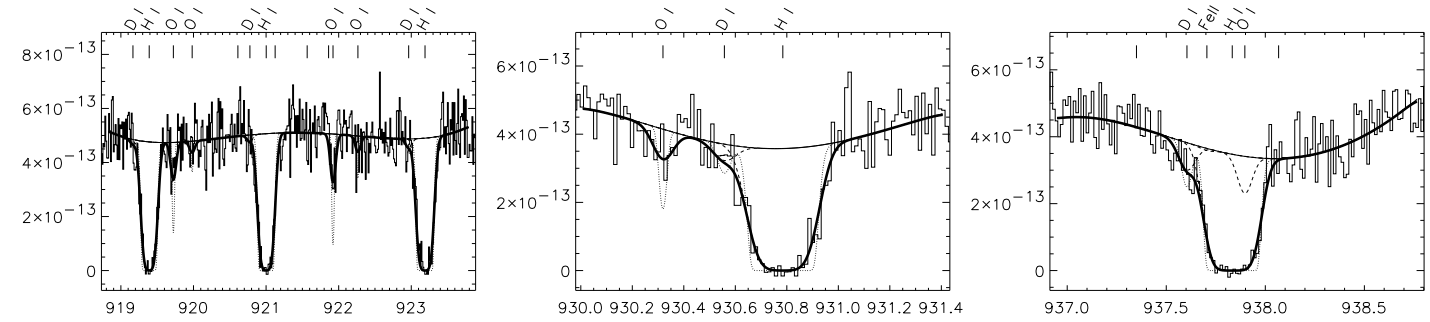

WD 2011+395

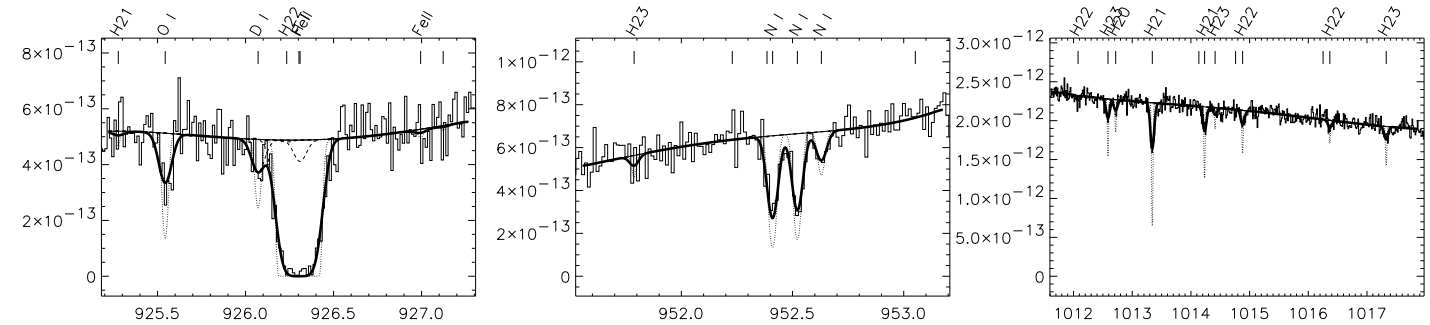

LB 1566

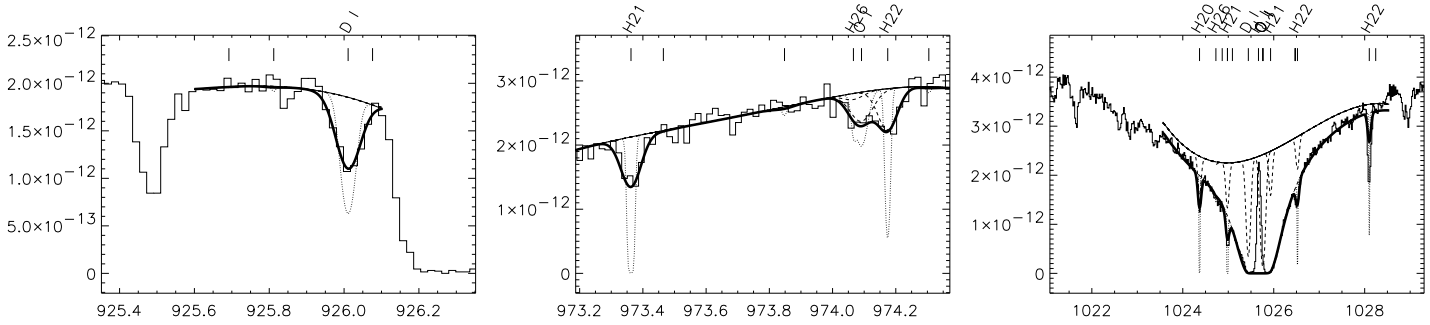

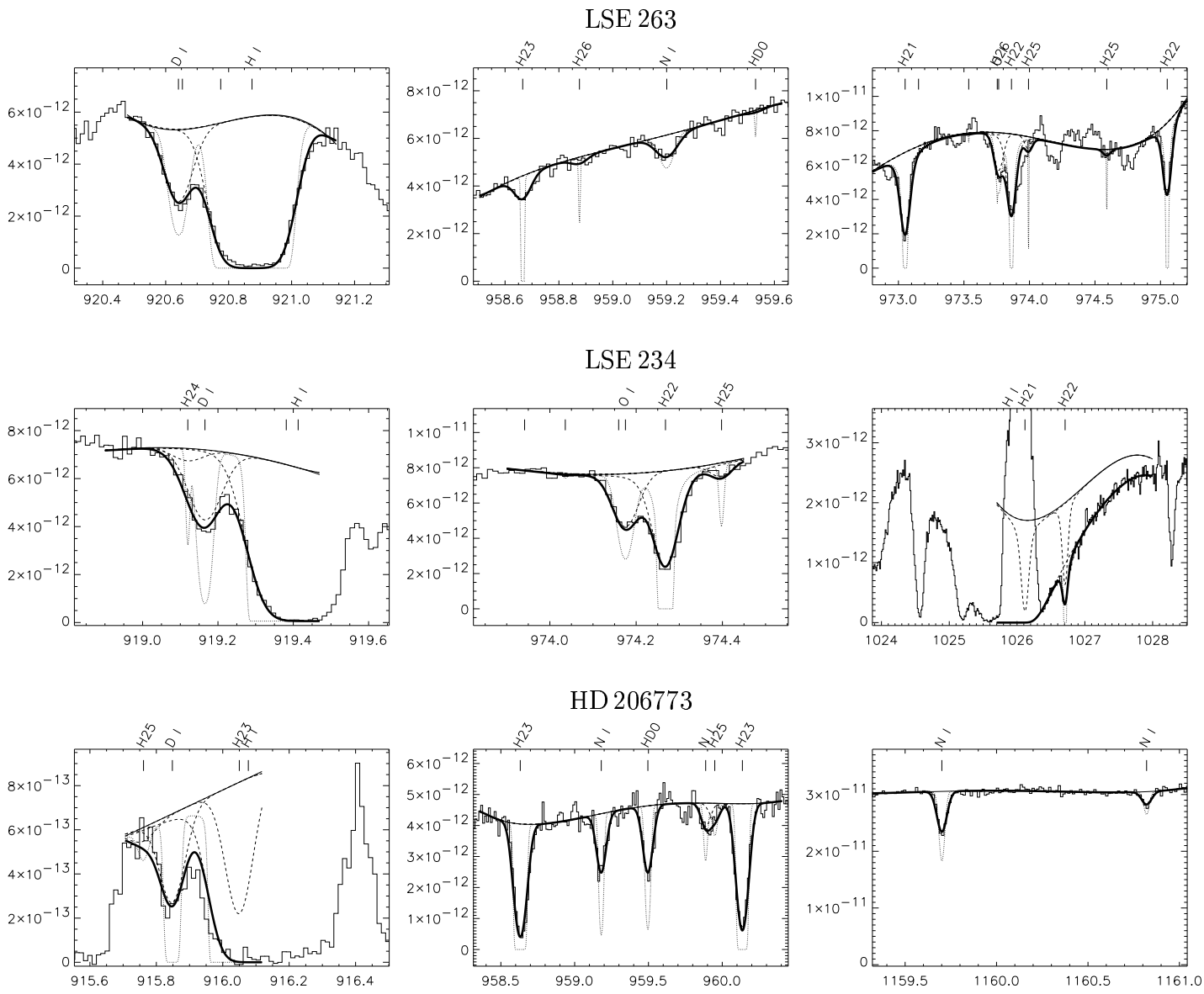

Figure 2: Examples of fits of the *FUSE* data toward the six targets. Histogram lines are the data, the solid lines are the fits (thick) and continua (thin). The dashed lines are the fits for each species. The dotted lines are the model profiles prior to convolution with the line spread function. The y-axis is flux in erg/cm^2/s/Å. The species are identified at the top of the plots for each line. The H_2 lines of the levels $J = 0$ to $J = 6$ are noted H20 to H26, and HD ($J = 0$) is noted HD0. The emission line in the center of the Lyman-β profiles is geocoronal.

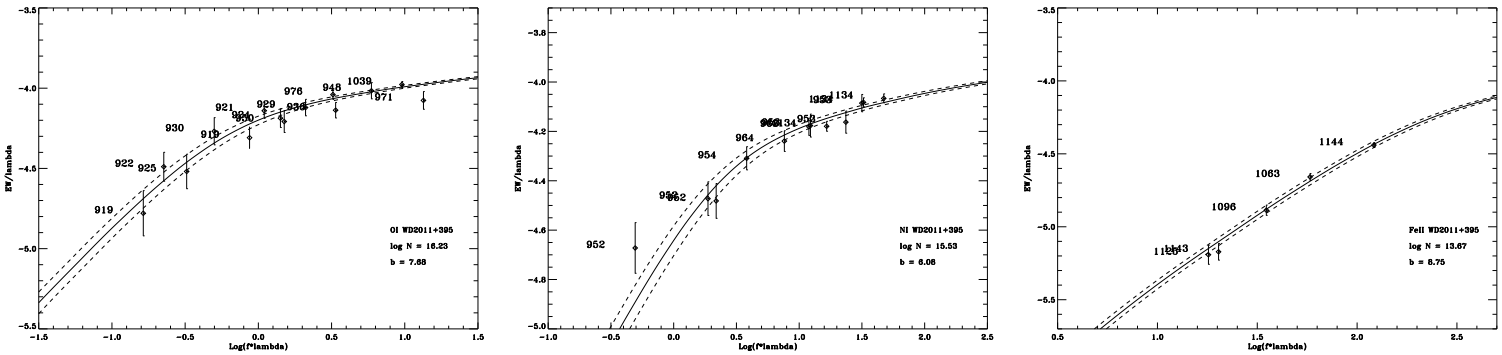

Figure 3: Fits of the curves of growth for O I, N I, and Fe II on the sight line to WD 2011+395.

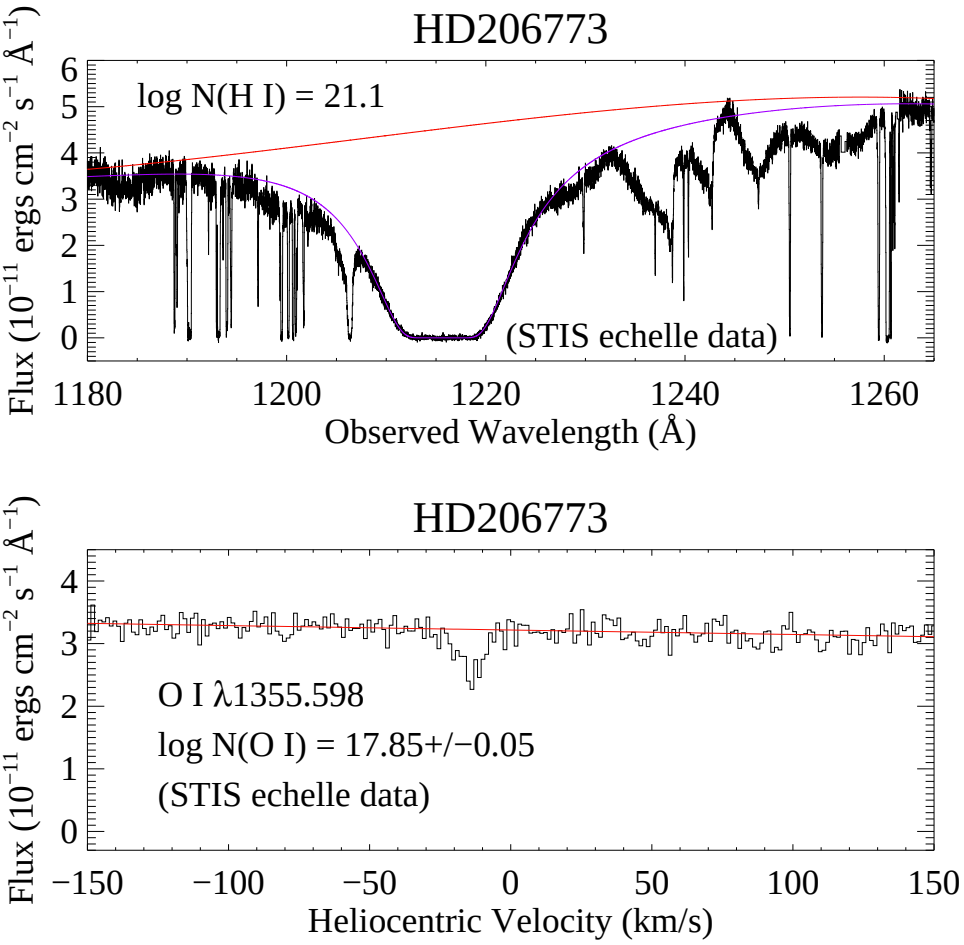

Figure 4: STIS data of Lyman-α and the O I line λ 1356 Å toward HD 206773. The assumed continua are overplotted in red. The blue line in the upper panel is the fit of the H I absorption. The O I absorption was directly integrated in order to measure N(O I).

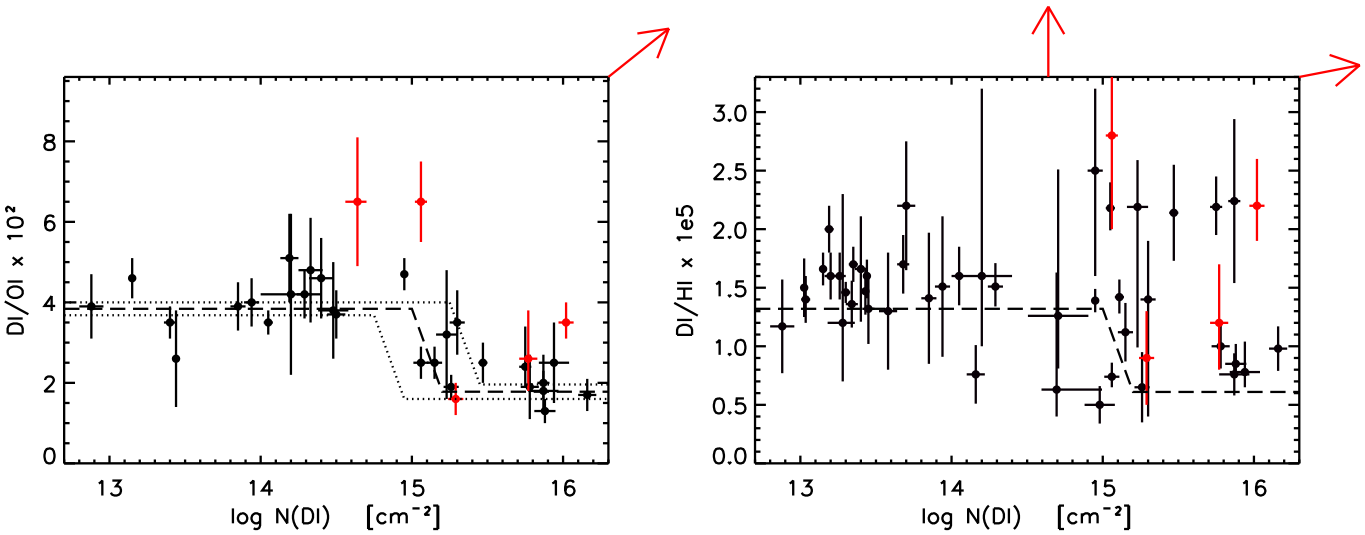

Figure 5: D/O (left) and D/H (right) as a function of $\log N(\mathrm{D\,I})$. The y-axes of the two plots are scaled to the same size, assuming $\mathrm{O/H} = 3.43 \times 10^{-4}$ (Meyer 2001). This figure is adapted from Hébrard et al. (2005), to which have been added LSE 44 (Friedman et al. 2006) and the six new targets presented on this poster (in red on the plot). The arrows indicate results falling out of the ranges of the plots, but with uncertain $N(\mathrm{D\,I})$ and/or $N(\mathrm{H\,I})$. The bimodal D/O picture presented by Hébrard et al. (2005) is overplotted with the dashed lines. All the error bars plotted here are $1\,\sigma$.

Table 2: Observations log.

Target	Obs. ID	Obs. date	Apert.[a]	$T_{\rm exp}$[b]	$N_{\rm exp}$[c]	Mode[d]	CalFUSE[e]
WD 1528+487	P2040101	2001 Mar 27	LWRS	17.8	12	TTAG	3.0.8
	D0580201	2004 Feb 26	MDRS	27.4	38	TTAG	3.0.8
			Total.....	45.2	50		
WD 2011+395	P2040401	2000 Nov 10	LWRS	11.5	4	TTAG	3.0.8
	M1053101	2002 Oct 29	LWRS	6.5	5	TTAG	3.0.8
	M1053102	2003 Oct 23	LWRS	12.9	9	TTAG	3.0.8
	D0580101	2003 Oct 21	MDRS	42.7	49	TTAG	3.0.8
			Total.....	73.6	69		
LB 1566	P3020801	2003 Jul 15	LWRS	5.0	2	TTAG	2.4.1
	P3020802	2003 Sep 11	MDRS	20.8	20	TTAG	2.4.1
			Total.....	25.8	22		
LSE 263	D0660401	2003 May 30	MDRS	4.0	8	HIST	3.0.8
	E0450201	2004 Sep 14	MDRS	23.1	32	HIST	3.0.7
			Total.....	27.1	40		
LSE 234	P2051801	2003 Apr 07	LWRS	8.9	19	HIST	2.4.0
	P3021101	2003 May 30	LWRS	10.6	18	HIST	2.4.1
			Total.....	19.5	37		
HD 206773	B0710901	2001 Jul 19	LWRS	4.4	8	HIST	1.8.7
	E0450101	2004 Sep 28	MDRS	27.7	58	HIST	3.0.7
			Total.....	32.1	66		

[a] LWRS and MDRS are respectively the large ($30'' \times 30''$) and medium ($4'' \times 20''$) *FUSE* apertures.

[b] Total exposure time of the observation (in 10^3 s).

[c] Number of individual exposures during the observation.

[d] HIST and TTAG are respectively histogram and time-tagged photon address *FUSE* modes.

[e] Version of the pipeline used for spectral extraction.

Table 3: Logarithms of the column densities (in cm^{-2}) and ratios (preliminary results).

Target	WD 1528+487	WD 2011+395	LB 1566	LSE 263	LSE 234	HD 206773
D I	$14.64^{+0.06}_{-0.08}$	15.06 ± 0.04	15.29 ± 0.05	15.77 ± 0.06	16.02 ± 0.05	17.0 ± 0.5
O I	$15.83^{+0.07}_{-0.06}$	16.25 ± 0.05	$17.09^{+0.07}_{-0.09}$	17.36 ± 0.15	17.48 ± 0.02	17.85 ± 0.05
N I	$15.13^{+0.06}_{-0.04}$	$15.52^{+0.04}_{-0.06}$	$16.02^{+0.08}_{-0.10}$	$16.62^{+0.03}_{-0.06}$	16.63 ± 0.03	17.204 ± 0.015
Fe II	$13.05^{+0.11}_{-0.14}$	13.69 ± 0.04	$14.68^{+0.08}_{-0.03}$	...	...	$15.05^{+0.04}_{-0.03}$
Si II	14.17 ± 0.10	$14.39^{+0.04}_{-0.02}$	...	...	...	...
P II	$12.46^{+0.08}_{-0.06}$	$12.65^{+0.04}_{-0.05}$	...	...	...	...
H I	$18.3^{+0.4}_{-0.6}$	$19.62^{+0.13}_{-0.16}$	20.35 ± 0.10	20.70 ± 0.15	20.68 ± 0.05	21.10 ± 0.05
H_2 ($J = 0$)	...	$13.29^{+0.04}_{-0.03}$	$14.63^{+0.08}_{-0.06}$	...	18.21 ± 0.10	...
H_2 ($J = 1$)	...	14.23 ± 0.02	$15.34^{+0.08}_{-0.07}$	...	18.35 ± 0.10	...
H_2 ($J = 2$)	...	13.65 ± 0.02	14.42 ± 0.03	...	17.36 ± 0.10	...
H_2 ($J = 3$)	...	$13.67^{+0.03}_{-0.02}$	14.06 ± 0.04	...	16.98 ± 0.10	...
H_2 ($J = 4$)	...	...	< 13.4	...	14.22 ± 0.20	...
H_2 ($J = 5$)	...	...	< 13.4	...	13.48 ± 0.40	...
H_2 (total)	...	14.45 ± 0.03	15.48 ± 0.09	...	18.62 ± 0.13	...
HD ($J = 0$)	...	...	< 13.6	...	...	14.77 ± 0.10
D/O $\times 10^2$	6.5 ± 1.6	6.5 ± 1.0	1.6 ± 0.4	$2.6^{+1.2}_{-0.8}$	$3.5^{+0.5}_{-0.4}$	14^{+30}_{-10}
D/N $\times 10^1$	3.2 ± 0.7	3.5 ± 0.5	1.9 ± 0.5	$1.4^{+0.3}_{-0.2}$	2.5 ± 0.3	$6.3^{+14}_{-4.3}$
D/H $\times 10^5$	22^{+65}_{-13}	$2.8^{+1.5}_{-0.8}$	0.9 ± 0.4	$1.2^{+0.5}_{-0.4}$	$2.2^{+0.4}_{-0.3}$	8^{+17}_{-6}
O/H $\times 10^4$	35^{+100}_{-20}	$4.2^{+2.2}_{-1.3}$	5.5 ± 3.0	$4.6^{+2.8}_{-1.8}$	6.3 ± 0.8	$5.6^{+1.0}_{-0.9}$
N/H $\times 10^5$	70^{+200}_{-40}	$7.9^{+4.2}_{-2.5}$	4.7 ± 2.1	$8.3^{+3.5}_{-2.6}$	8.9 ± 1.2	$12.7^{+1.6}_{-1.4}$
log P II/O I	-3.37 ± 0.10	-3.60 ± 0.07	...	...	...	...
$f(H_2)$	...	2×10^{-5}	3×10^{-5}	...	2 %	...
HD/D I	...	...	< 2 %	...	...	~ 1 %
Target	WD 1528+487	WD 2011+395	LB 1566	LSE 263	LSE 234	HD 206773

All the error bars are 1σ.